Advancements in Capacitive Touch System and Stylus Technologies

Ha-Min Lee and Seung-Hoon Ko

Department of Electronic Materials Engineering, Kwangwoon University, Seoul 01897, Korea

Abstract: Due to changes in the form factor of display panels and touch screen panels in various devices, capacitive touch systems have evolved to address various issues such as low power consumption, noise immunity, and small chip size. Furthermore, some devices have applications that use a stylus. Since the stylus operates similarly to a finger touch, it encounters similar issues. Recent research trends focus on addressing key issues such as noise, which is primarily caused by the self-capacitor formed between the display cathode and the touch screen panel. In this paper, Various research papers discussing methods to eliminate external noise will be reviewed. These advancements enhance noise immunity in touch systems, making it easier to use thinner and more flexible panels. These progress make touch technology more versatile and reliable in various applications.

Keywords: Touch screen panel, Analog front-end, Capacitive touch system, Stylus, Signal to noise ratio, Readout circuit

1. INTRODUCTION

Today, touch systems are used in various applications such as smartphone, tablet PCs, and all-in-one computers. These touch systems have evolved through various sensing methods, including acoustic, resistive, optical and capacitive. Among these, the capacitive method is more suitable for advanced technology due to its high sensitivity and multi-touch capabilities.

In a capacitive touch system (CTS), a touch screen panel (TSP) is required to detect finger touch [1]. As illustrated in Fig. 1(a), TSP has two electrodes, a transmitter (TX) and a receiver (RX), which intersect perpendicularly. As shown in Fig. 1(b) and (c), CTS can be classified into two sensing methods: self-capacitor (C_S) and mutual-capacitor (C_M) sensing to detect finger touches. C_S refers to the capacitor between either the TX or RX electrodes and ground plane, while C_M denotes the capacitor formed between TX and RX electrodes. When a conductive finger or capacitive stylus approaches the display, capacitive changes occur in both C_S and C_M. In the case of C_S, the finger capacitor ΔC_S is connected in parallel with existing C_S, thus increasing the total capacitance between the electrode and ground. For C_M, the fringing field of C_M is disrupted by the finger, decreasing C_M by the amount of ΔC_M. Thus, self-capacitance and mutual-capacitance are composed of static and dynamic components. The static components of C_S and C_M, are a type of offset capacitance which doesn't change whether the sensing node of the TSP is touched or not. The ΔC_S and ΔC_M are dynamic components that vary when TSP is touched. The static component offset, occupying a large portion of the sensing signal, can lead to analog-front end (AFE) saturation. Thus, an additional method to compensate for this static component is necessary, which amplifies the dynamic component while

✉ Seung-Hoon Ko; shko@kw.ac.kr

reducing the static component, thereby improving the detection of touch presence.

In the case of the TSP, as shown in Fig. 2, it has evolved from an add-on type placed on top of the display panel to on-cell and in-cell types integrated with the display panel [2]. The integration of display panels and TSP offers advantages in terms of thickness, transparent and cost-efficiency, making it suitable for recent flexible and stretchable products. Despite the advantages of integrating TSP and display panel, it has the drawback of increasing the C_s capacitance. The increase in C_s leads to various issues, such as increased display noise, AFE signal saturation and limited TSP bandwidth [3].

In CTS, the signal-to-noise (SNR) is an important figure that characterizes noise performance. There are various external noise sources such as display noise, chargers, fluorescent lights and human noise. Among these, the impact of display noise becomes more significant as the C_s capacitance increases. Display noise exhibits a common-noise characteristic that is uniformly distributed across all TSP regions. To mitigate such common-noise sources, differential sensing schemes [4-6] are commonly employed, which will be explained in Section 2.1. Compared to capacitive finger touch, various types of styluses are used to obtain coordinate information for stylus touch.

Stylus can be broadly categorized into passive and active types. Passive stylus includes capacitance (C)-type, electromagnetic resonance (EMR) type, and electrically coupled resonance (ECR) type styluses while the active type includes C-type active stylus. Table 1 summarizes the advantages and disadvantages of each type of stylus. Unlike other styluses, the passive C-type does not require additional circuitry or panels, offering benefits in terms of complexity and cost [7]. In the case of EMR, it has the advantages of being able to represent high-resolution pressure and tilt. However, it has drawbacks such as higher fabrication cost, increased thickness of display panel, and higher power consumption due to the additional EMR sensor layer onto the display [8]. ECR does not require an additional sensor layer but can only achieve low-resolution sensitivity [9,10], since it is also affected by capacitively coupled noises similar to the capacitive TSP system. The C-type active stylus has the advantage of being able to express pressure and tilt with high sensitivity. However, it has the drawback of increased production costs due to the need for additional circuitry and a
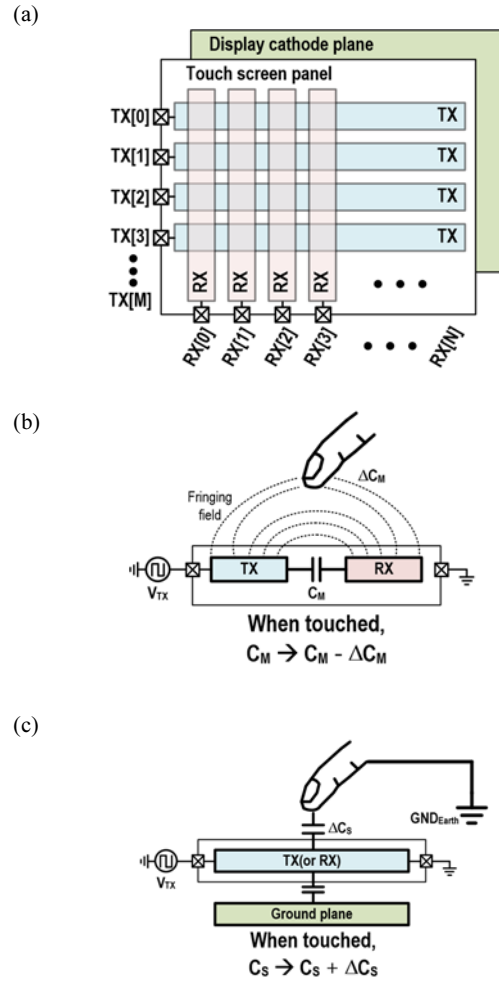

Fig. 1. (a) TSP structure with M TX × N RX electrodes, and conceptual diagrams illustrating, (b) mutual-capacitance sensing, and (c) self-capacitance sensing methods.
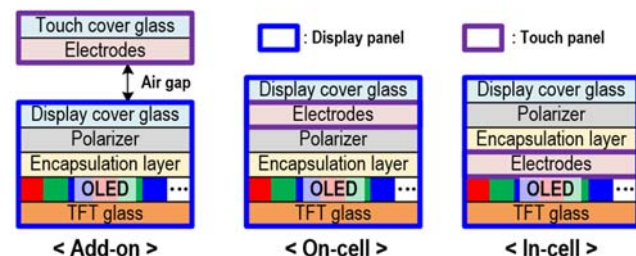

Fig. 2. Types of TSPs in OLED.

rechargeable battery in the stylus [11-13].

In this paper, recent research related to styluses is discussed. Section 2 describes the main AFE architecture, section 3

**Table 1.** Types of stylus and their characteristics.

Types	C-type passive stylus	EMR-type passive stylus	ECR-type passive stylus	C-type active stylus
Battery	No	No	No	Yes
Additional sensor	No	Yes	No	No
Fabrication cost	Low	High	Low	High
Sensitivity (SNR)	Low	High	Middle	High
Pressure	No	Yes	Yes	Yes
Tilt angle	No	Yes	No	Yes
Stylus cost	Low	Low	Low	High

covers the operation of each type of stylus, and section 4 explains the research conducted on solutions to various issues. Finally, the conclusion is given in section 5.

2. CAPACITANCE SENSING AFE

2.1 Basic touch sensing architecture

Generally, capacitive-sensing AFE has the process of converting capacitance signal into an electrical voltage. As shown in Fig. 3(a), the sensing capacitors (C_M or C_S) are driven by V_{TX} represent the series resistance of each TX and RX electrode, and i_X and i_Z denote the input and output currents of CCII, respectively. Moreover, the CCII has the characteristic of copying the or V_{drv}. The charge proportional to C_M or C_S is then accumulated on C_{INT}—and converted into a corresponding voltage, V_{OUT}—. However, conventional AFE architecture suffers from limited bandwidth, particularly as C_S increases in flexible displays due to the reduced distance between the TSP electrode and ground plane. Therefore, recent AFE designs employ a second-generation current conveyor (CCII), which separates the capacitance to voltage conversion (Q-to-V) from the high capacitive-load TSP, as shown in Fig. 3(b). In this figure, $R_{P,TX}$ and $R_{P,RX}$ input current with a gain of G ($i_Z = G i_X$). Since G is included in the output voltage formula, the AFE gain can be adjusted accordingly. As shown in Fig. 4(a), in a conventional AFE that do not include a CCII, the bandwidth is determined by the open-loop gain unity gain bandwidth (UBW) multiplied by (C_{INT}/C_S). As C_S increases, it becomes
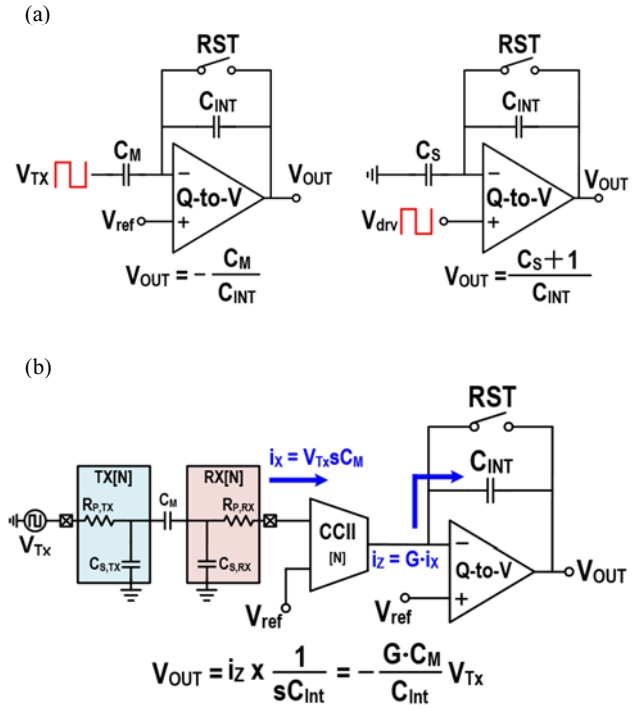
Fig. 3. (a) Conventional TSP's AFE architecture and (b) AFE with second generation current conveyor.
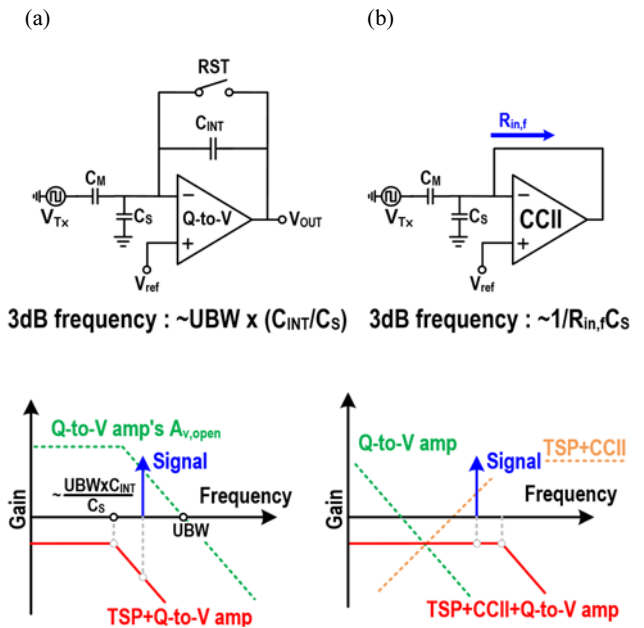
Fig. 4. (a) The frequency response of the AFE without CCII and (b) the frequency response of the AFE with CCII.

difficult to achieve the proper gain at the signal frequency. On the contrary, when using CCII at the first stage of AFE, the bandwidth can be increased by minimizing the input feedback resistance ($R_{in,f}$) of the CCII, as shown in Fig. 4(b). Therefore, the AFE can operate with a high-frequency V_{TX} or V_{drv}, leading to an increased frame rate.

2.2 Differential sensing

In recent TSP readout systems, the increased display noise due to the thin display stack-up has become a significant issue. To mitigate this, differential sensing between adjacent RX electrodes can effectively eliminate common display noise. As shown in Fig. 5(a), differential sensing works by subtracting the capacitance signals (C[N]-C[N+1]) of two adjacent RX electrodes, removing common noise (N_{CM}) at the output.

Fig. 5(b) shows an implementation example of differential sensing using the aforementioned CCIIs and Q-to-V converters, where differential capacitance (C[N]-C[N+1]) is measured with gain adjustment of two CCIIs, while effectively eliminating common noise N_{CM}.

However, as shown Fig. 6(a), obtaining an accurate touch profile requires digital reconstruction process, which restores differential capacitance data into single-ended data of each
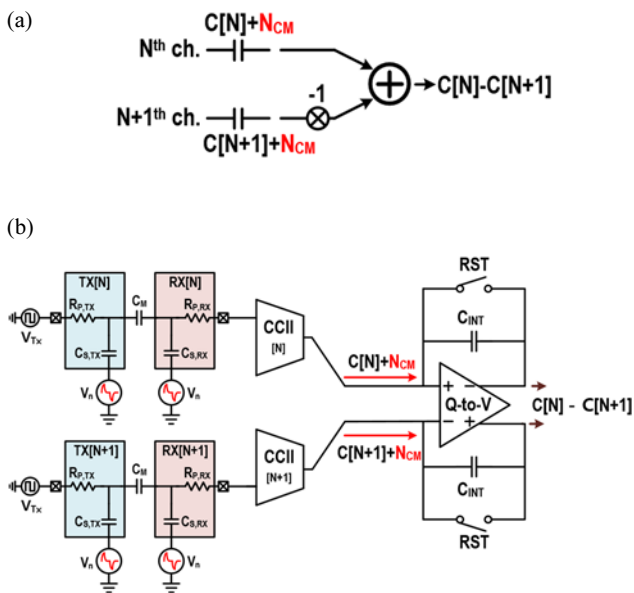
capacitance node. Given that differential values are obtained between RX electrodes, integration must be performed across the TSP channels of the RX electrodes, based on the integral constant $C_{S[0]}$. Since $C_{S[0]}$ must be obtained through single-ended sensing, this data also becomes highly susceptible to noise ($C_{S[0]}$+Noise) unless an additional noise-filtering strategy is applied. Another differential sensing method is the pseudo-differential method [4], where the capacitance from an unused TSP electrode ($C_{S,D}$) is employed to act as a reference channel [Fig. 6(b)]. The $C_{S,D}$ is subtracted from all other TSP channels to remove the common noise. In this case, the static component of the sensing capacitor can also be effectively removed by the unchanged $C_{S,D}$. Furthermore, it has the advantage that there is no need for digital reconstruction to restore original data. However, due to the significant phase delay from the RC component of the TSP in recent flexible displays, inconsistencies in display noise occur at each capacitance node, which degrades the effectiveness of differential noise cancellation.
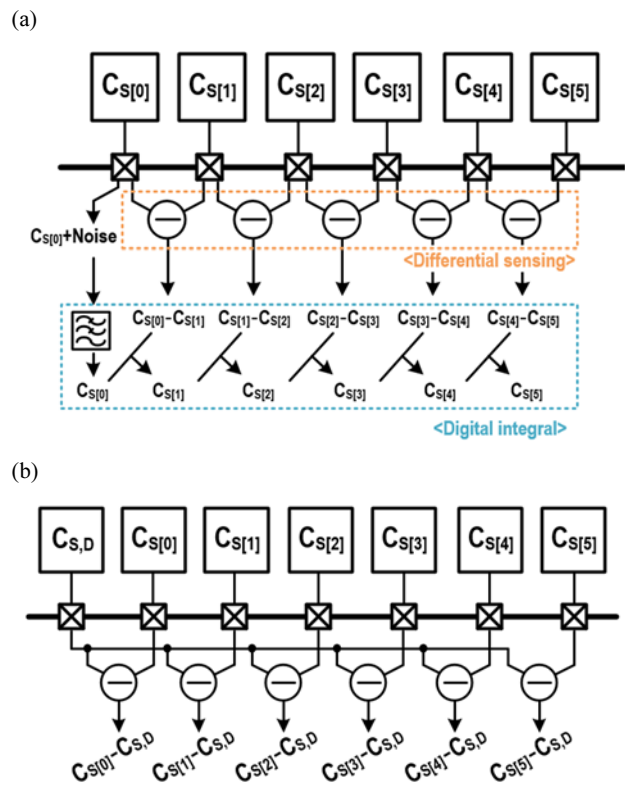
(a)

(b)

(a)

(b)

Fig. 5. (a) Conceptual diagram of the differential sensing scheme and (b) practical differential sensing AFE architecture.

Fig. 6. (a) Simplified diagram of the differential sensing and (b) pseudo-differential sensing.

3. TYPES OF STYLUS

3.1 C-type passive stylus

The C-type passive stylus has been widely used in the CTS due to its light weight and low manufacturing cost. The C-type passive stylus operates in a manner similar to a finger touch. Figure 7 shows a conceptual diagram of the C-type passive stylus. When the stylus approaches the display, it causes a capacitive variation in both TX and RX electrodes of the TSP, subsequently measured by the AFE. To increase the capacitance variation by the stylus, the contact area between the stylus and the display needs to be increased. Nonetheless, in the case of a C-type passive stylus, the contact area is significantly less than that of a finger touch, resulting in reduced signal amplitude and consequently decreased SNR and lower stylus touch accuracy. Furthermore, the C-type passive stylus does not support additional features such as pressure sensing and tilt angle detection.

3.2 Electromagnetic resonance (EMR) stylus

The EMR stylus can detect pressure, tilt angle and button actions. Figure 8 shows a conceptual diagram of the EMR stylus. In order to detect the EMR stylus, an additional layer consisting of a magnetic coil must be added to the existing display stack-up. When the coil is driven by the EMR excitation circuit and SW1 is on, current flows through the

magnetic coils of the panel, creating a magnetic field around the stylus. Then, the stylus stores the signal of the resonance frequency according to the following formula:

$$f_{styus} = \frac{1}{2\pi\sqrt{L_{TANK} \times (C_{TANK} + C_{PRESSURE} + C_{BUTTON})}} \quad (1)$$

The tank inductor (L_{TANK}), tank capacitor (C_{TANK}), pressure-sensitive capacitor ($C_{PRESSURE}$), and button capacitor (C_{button}) are the components of the equivalent circuit of the stylus (Fig. 8).

$C_{pressure}$ uses a variable capacitor that changes with the pressure applied by the pen, thereby altering the total capacitance. The button can also modify the total capacitance by connecting or disconnecting C_{button} through a switch, depending on whether the button is pressed or not. When the SW1 is off and SW2 is connected, the current flowing through the magnetic coils of the EMR panel stops, and the signal of the resonance frequency is transmitted from the stylus to the EMR panel. Therefore, by sensing the changes in the value of the button and pressure capacitor, the signal frequency sent to the EMR readout varies, allowing for the detection of pressure and button actions. EMR stylus requires an additional EMR magnetic panel compared to other styluses. This leads to higher power consumption, increased thickness of the display panel, and higher fabrication costs. Furthermore, EMR styluses are significantly influenced by the density and uniformity of the magnetic coil, which is a notable drawback.
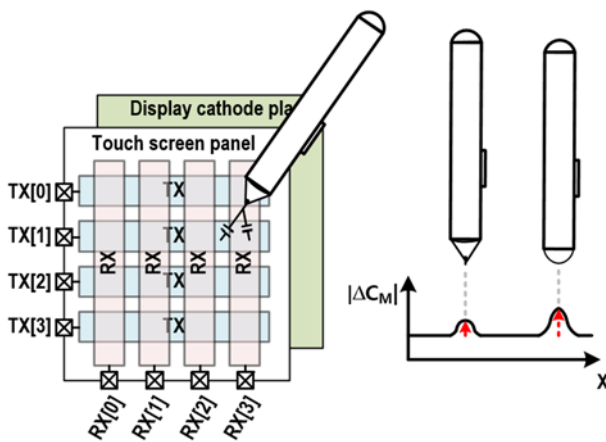

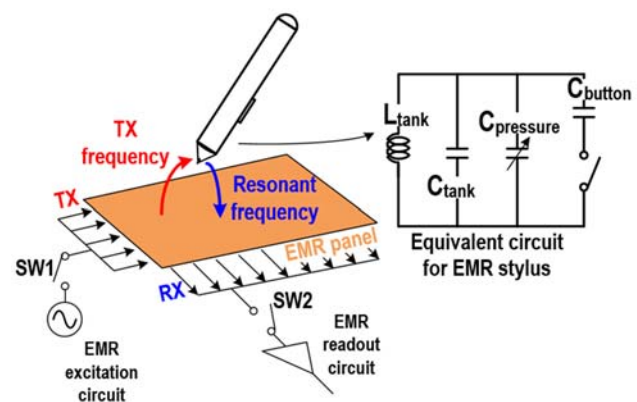**Fig. 7.** Conceptual diagram of the C-type passive stylus.

Fig. 8. Conceptual diagram of the EMR stylus.

3.3 Electrically coupled resonance (ECR) stylus

While EMR sensing requires an additional magnetic coil layer, resulting in increased thickness and power consumption, the ECR sensing does not require an additional layer in the display. Figure 9 shows the ECR stylus structure with an equivalent circuit, similar to that of the EMR. The stylus can be represented by an equivalent circuit of tank inductor (L_{tank}) and the pressure capacitor ($C_{pressure}$). In the AFE excitation circuit, the excitation signal is transmitted to the stylus via TX, and a specific resonant frequency signal determined by L_{tank} and $C_{pressure}$ is trans mitted to RX. The resonance formula is as follows:

$$f_{sty} = \frac{1}{2\pi\sqrt{L_{tank}C_{pressure}}} \tag{2}$$

So, similar to the EMR, resonance frequency is varied by the $C_{pressure}$. Finally, the signal is transmitted from RX electrode (RX[N]) to the AFE readout circuit, indicating stylus's location. Unlike the EMR stylus, where energy is transferred in the form of magnetic energy, the ECR stylus transmits signals through the capacitor formed between the stylus and TX (C_{TS}) and the capacitor formed between stylus and RX (C_{RS}). Due to the small capacitive couplings of C_{TS} and C_{RS}, the amplitude of the transmitted signal is small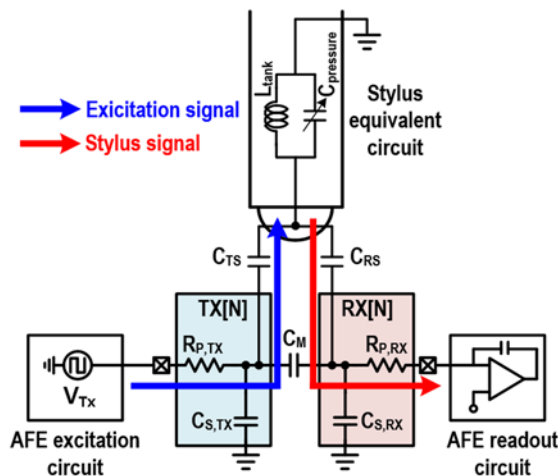er compared to EMR. Therefore, ECR has the drawback of being vulnerable to weak signal strength and reduced SNR. This requires high-voltage excitation from the AFE, which result in increased power consumption and chip size, posing additional design challenges for the AFE.

3.4 C-type active stylus

Passive styluses have the advantage of low fabrication cost, but they suffer from low signal levels, leading to low SNR. To address this, EMR stylus has been used. But they introduce issues in thickness and fabrication cost due to the additional panel required. Active stylus has gained interest to solve these problems. The active stylus contains several IC and additional sensors. Therefore, it requires a rechargeable battery. As shown in Fig. 10, the force gauge is included to measure pressure, and a gyro sensor is included to detect the tilting angle. Based on these information, an excitation signal is generated by the excitation circuit, and the signal is transmitted to the TSP through the thin tip of stylus. Since the stylus independently generates signals and sends them to the TSP, the signals from the stylus need to be distinguished from the signals for finger touches. To achieve this, synchronization between the active stylus and the AFE must be carried out, and an IC for data communication needs to be included in the active stylus. In the case of an active stylus, it has advantage of high sensitivity compared to passive stylus because it directly generates the signals and sends them to TSP. Therefore, active stylus has advantage in hovering. Additionally, the active stylus also has advantages of being able to express pressure and tilt angle. However, as various components are included inside the stylus, there are issues such as an increase in the thickness and weight of the stylus, high power consumption due to the use of a battery, and an increase in fabrication cost due to the increased complexity of the stylus.
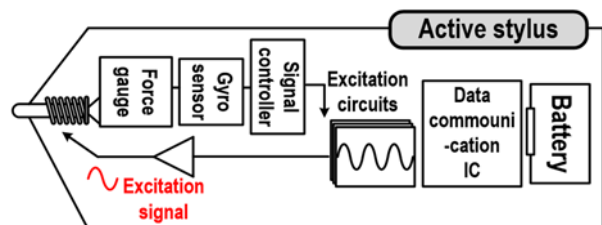

Fig. 9. Conceptual diagram of the ECR.

Fig. 10. The diagram of the components of the active stylus.

4. RECENT AFE ISSUES FOR STYLUS

4.1 Noise reduction method

In designing AFE, various issues arise, with noise rejection being considered the most critical. To increase SNR, the commonly used method in CTS is code-division multiple sensing method (CDMS) [9,13,14]. As shown in Fig. 11(a), When channels driven in parallel, their capacitance information goes into a single AFE. The encoding process applies coefficients of 1 or -1 to the driving signals. As depicted in Fig. 11(b), using coefficients for the codes, we obtain data from time T1 to time T4. After passing through the AFE it's possible to extract information that contains each capacitance of the TX1~4 by decoding process. In contrast to the time-interleaved method where each TX senses separately,

CDMS offers the advantage of reducing sensing time by a factor of N which is the length of the code sequence. Given the mutual sensing time, reducing time by factor of N in CMDS leads to an increase in SNR a factor of $\sqrt{N}$.

CDMS can also be applied similarly in active stylus sensing. However, the problem when using such code sequences lies in the synchronization between the excitation signal for finger touch and the excitation signal for the active stylus. Therefore, to address both the synchronization issue between the stylus and AFE and the SNR issue, the multiple-frequency driving method (MFDM) has been proposed [10]. As shown in Fig. 12(a), there are TSP, stylus, AFE blocks, and additionally the fast fourier transform (FFT) processor is included. MFDM involves using signals at different frequencies can be separated and analyzed. The switch with a select signal is used between the AFE's readout and the excitation circuit. This witch alternates, sequentially sensing the stylus's x and y coordinate information. Initially, when no signal is incoming, FFT processing is conducted.

As illustrated in Fig. 12(b) performing FFT when no signal is present allows obtaining the spectrum of external noise. Based on this data, the MCU identifies low-noise regions and communicates the frequency ranges of signals to be used by the stylus through wireless communication. The gray region allows allocating the frequency bands of driving signals from AFE's channel 1 to N, and assigns the frequencies for stylus use in the other three regions. The reason for using three signals in the stylus is because the data to be sent from the stylus to the AFE includes the stylus's position, pressure and tilt angle. When stylus coordinate information f_{S1} detected by the AFE, it indicates the presence of the stylus in the corresponding channel. For pressure and tilt angle, the information must be provided according to the degree of pressure and tilt angle. Therefore, when the force gauge or gyro sensor detects pressure and tilt angle, processing is needed to vary the signal frequency according to the degree of these measurements. The signals f_{s2} and f_{s3}, which represent pressure and tilt angle, have Δf_{s2}, Δf_{s3}. The resolution of pressure and tilt angle is determined by how the Δf_{s2}, Δf_{s3} are distributed within their respective ranges.

In CDMS, as the code length increases, it leads to an increase in column offset, which can cause the AFE to saturate. Therefore, the usable code length is generally limited. Consequently, as the number of channels in the TSP increase,
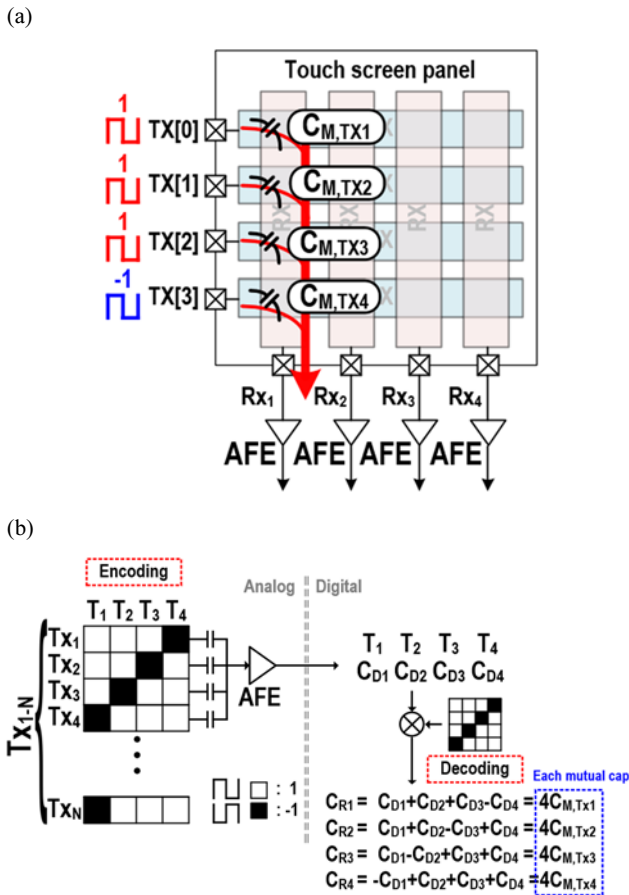
(a)

(b)

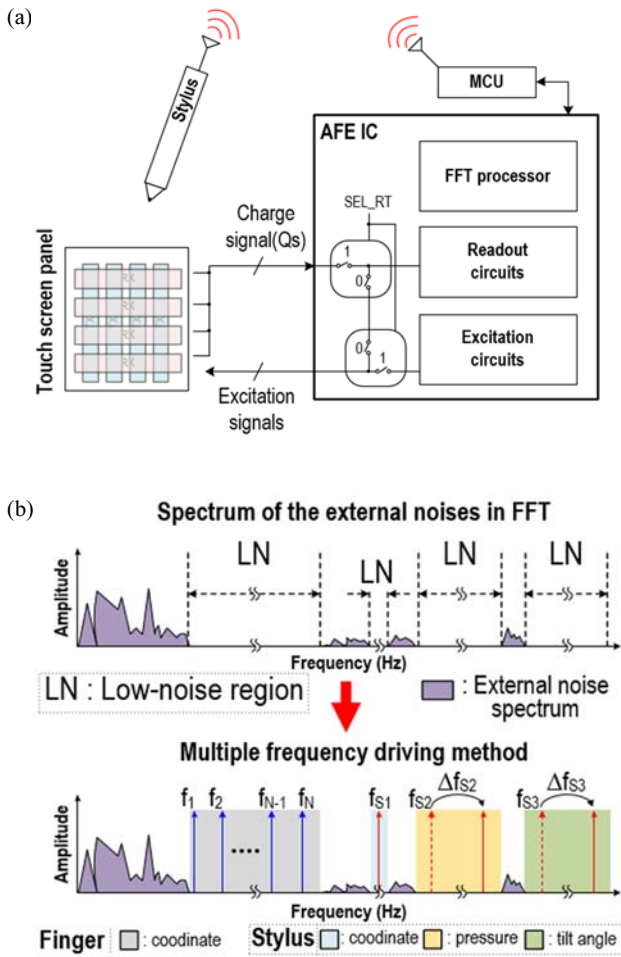**Fig. 11.** (a) CDMS of 4×4 TSP and (b) diagram and mathematical expressions of encoding and decoding.

(a)

(b)

Fig. 12. (a) Block diagram of the CTS and (b) operational principle of the multiple-frequency driving method.

(a)

(b)

Fig. 13. (a) Charge overflow problem with N channels and (b) amplitude-modulated multiple-frequency excitation.

CDMS eventually has to implement time-interleaved iterations. Therefore, with a larger number of channels, MFDM can be advantageous in terms of SNR because it allows all channels to be driven simultaneously at different frequencies. However, since all channels are driven simultaneously, there is a phenomenon where a significant amount of charge enters the AFE at specific timings [11]. This is known as the charge overflow problem. As shown Fig. 12(a), when all channels of the N-channel TSP are driven simultaneously, the excitation signals from channel <1>, $V_{EXT<1>}$, to the excitation signal of the Nth channel, $V_{EXT<N>}$, are injected into a single AFE. There is a phenomenon where the amount of charge from all channels peaks periodically. This phenomenon occurs at the beat frequency period. The MCU then checks the distribution of the excitation signal
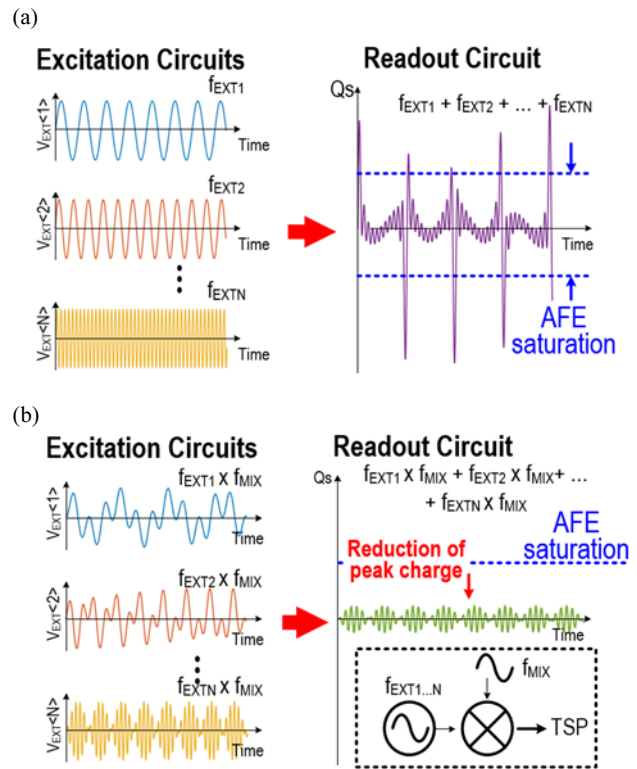
frequencies from f_{EXT1} to f_{EXTN} and determines the beat frequency. Subsequently, it mixes the beat frequency into all the excitation signals. As shown in Fig. 12(b), the mixing process reduces the charge peak amplitude and this process is referred to the amplitude-modulated multi-frequency excitation method (AM-MFE). the excitation signal. This contributes to a higher SNR.

AM-MFE involves a signal modulation process, so an accurate Using AM-MFE processing not only prevents AFE saturation by charge overflow but also allows for a greater amplitude of data recovery process is necessary. As shown in Fig. 13, assuming the signals' frequencies from f_{EXT1} to f_{EXTN} are distributed with a frequency difference of f_d, the f_{MIX} signal is used with the same frequency as $f_d/2$. After modulation, signal mixing occurs, resulting in $f_{EXT} + f_{MIX}$ and $f_{EXT} - f_{MIX}$ signals. At this point, the $f_{EXT1} + f_{MIX}$ and $f_{EXT2} - f_{MIX}$ signals cancel each out. This cancellation happens similarly with the subsequent signals, leaving only the $f_{EXT1} - f_{MIX}$ and $f_{EXTN} + f_{MIX}$ signals, with the remaining signals summing to zero. The $f_{EXT1} - f_{MIX}$ can be recognized as f_{EXT1} data. Subsequently,
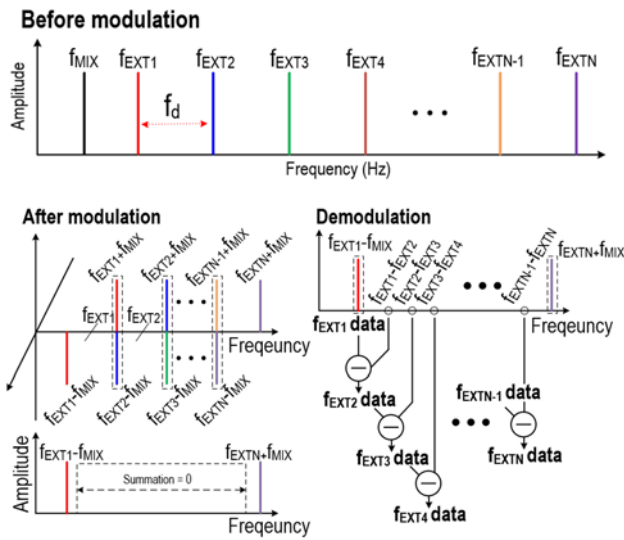
Fig. 14. The process of modulation and demodulation of a signal.

similar to the digital integration of a differential signal, continuously adding the f_{EXT1} - f_{MIX} signal allows the recovery of the remaining excitation signal values. This method has the advantage of reducing the calculation load compared to the conventional method of remixing to restore the original signal. Therefore, the load on the MCU is reduced.

In paper [4], adjustable frequency modulation (AFM) and linear interpolating data reconstruction (LIDR) are proposed to prevent external noise from the palm. Figure 15 shows the process of the noise suppression with AFM and its architecture. The fluorescent lamps, chargers, and hum noise mostly exists in the low-noise region, ranging 20 to 250 kHz. Additionally, their harmonics are located in the high-frequency region, above 700 kHz. Therefore, noise is present around the signals we use. Although a band-pass filter is the most effective for removing this noise, adjusting the cut-off frequency of a band-pass filter is not straightforward. In the AFM method, the AFE includes a down-conversion block. This down-conversion block modulates the signals we use to a frequency of f_{mod} - f_{PEN} while modulating the external noise to high frequencies. In Fig. 16, it is implemented with a simple switch mixer. Afterwards, the high-frequency modulated external noise is suppressed using low-pass filtering. The signal is then appropriately amplified for use by programmable gain amplifier (PGA). When modulating the signal into the low noise in this way, an additional technique called LIDR can be employed. As illustrated in Fig.16, during each horizontal
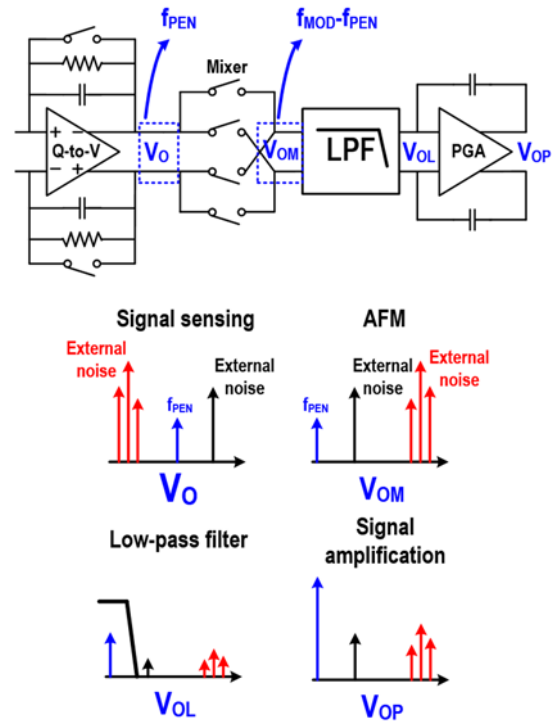

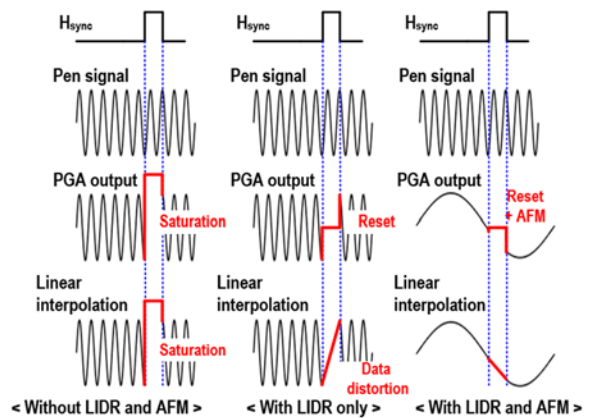
Fig. 15. AFM architecture and process.

Fig. 16. Time domain analysis of the LIDR and AFM.

sync (H_{sync}) of the display panel, capacitive-coupled noise is transmitted to the AFE, which can lead to AFE saturation. If the signal frequency during linear interpolation exceeds that of the H_{sync}, the signal may not be properly recovered. Therefore, AFM resolves this issue by modulating the signal frequency to a lower frequency range. Data reconstruction through linear interpolation is more accurate when AFM is used in together with LIDR compared to when AFM is not used.
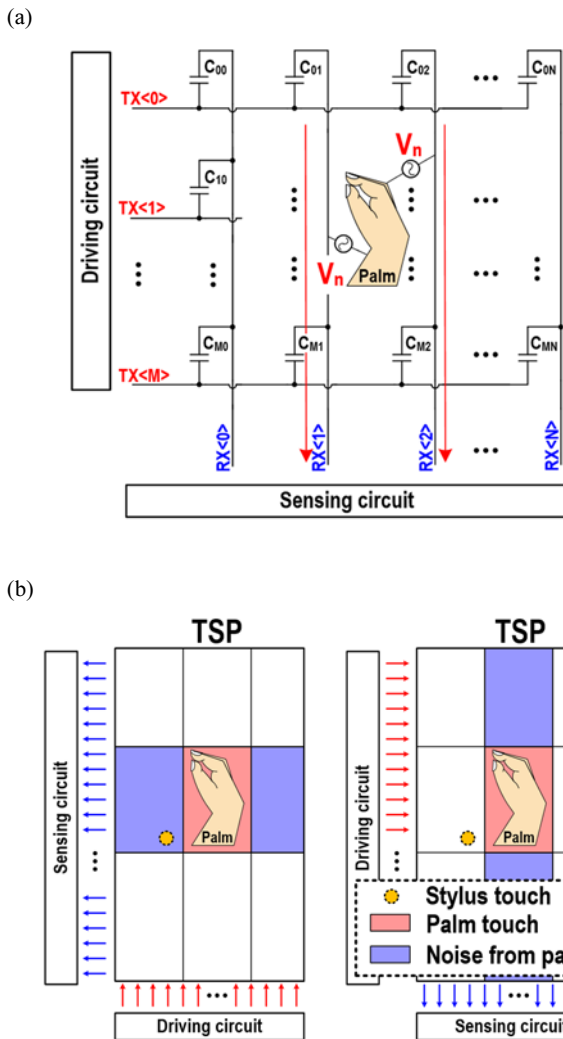
(a)

(b)

Fig. 17. (a) The TSP architecture and noise injection model and (b) alternating driving method.

Fig. 18. Additional signal, V_{palm}, for the palm rejection in the active stylus.

4.2 Palm rejection method

Unlike finger touch sensing, a key issue that arises with stylus usage is palm detection. When drawing on the display with a stylus, the palm of the hand holding the stylus usually touches the display. Since this is an unintended touch, the CTS needs a function to reject such palm touches. Additionally, as shown in Fig. 17(a), in the case of a passive stylus, the signal from the stylus is relatively weak. This present the problem where the stylus signal can be buried by noise transmitted from the palm stylus system. To address this issue, as shown in Fig. 17(b), a method of alternating the direction of driving and sensing is sometimes used. Another approach is a palm
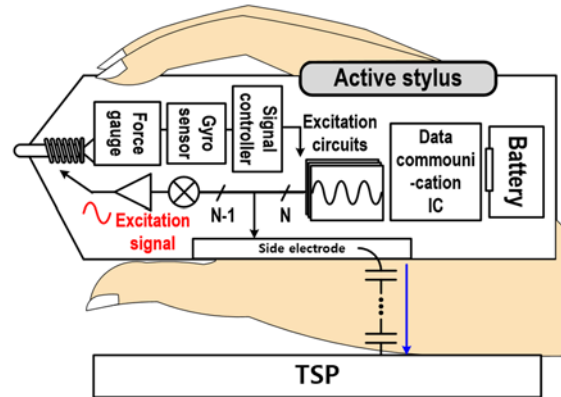
detection filter [15]. This method assumes the peak point in the obtained data as the touch point and checks the surrounding data to determine how much touch has occurred. By using a predetermined threshold (TH_{base}), it verifies how much data within a specific surrounding distance exceeds this threshold. Then, by using the number of threshold (TH_N), if the number of data points exceeding TH_{base} is greater than TH_N, it is considered a palm touch. Therefore, to determine the presence of palm touch using the palm detection filter, it is important to set appropriate values for TH_{base} and TH_N, as well as to determine the extent of the data surrounding the peak data to be analyzed.

In an active stylus system, an additional palm excitation signal can be used to differentiate palm touches [12]. When generating the excitation signal in the active stylus, an additional V_{palm} signal with a frequency of f_{palm} is crated. By ensuring that the V_{palm} signal is transmitted from the stylus side electrode through the hand to the palm and then to TSP, the AFE can sense the V_{palm} signal at the coordinates where the palm is touching. Subsequently, this signal can be identified by FFT as a palm touch and rejected, thereby implementing the palm rejection.

5. CONCLUSION

CTS are crucial in modern devices like smartphones and tablets due to their sensitivity and multi-touch capabilities. They utilize TSP, which offer thinner and cost-efficiency. However, integration of TSP and display panel can increase

self-capacitance, leading to challenges such as noise and reduced signal sensitivity.

Advanced AFE architectures, including CCII and differential sensing methods, effectively mitigate these issues. They enhance SNR and touch accuracy. Techniques like CDMS and MFDM further enhance noise reduction and prevent synchronization problem, particularly beneficial for active stylus systems.

Stylus technologies, whether passive or active, continue to advance with distinct advantages such as sensitivity, cost-effectiveness, and additional features like pressure and tilt detection. Integrated with sophisticated AFE designs, these styluses ensure precise and responsive touch interactions.

Overall, ongoing innovations in CTS and AFE technologies promise continual improvements in touch system performance, driving the development of more intuitive and efficient touch-enabled devices.

ORCID

Seung-Hoon Ko   https://orcid.org/0000-0001-6018-1104

REFERENCES

[1] J. M. Lee, J. W. Ham, W. S. Jang, H. M. Lee, S. M. Koo, J. M. Oh, and S. H. Ko, *J. Korean Inst. Electr. Electron. Mater. Eng.*, **36**, 423 (2023).
doi: https://doi.org/10.4313/JKEM.2023.36.5.1

[2] O. K. Kwon, J. S. An, and S. K. Hong, *IEEE Sens. J.*, **18**, 4832 (2018).
doi: https://doi.org/10.1109/JSEN.2018.2830660

[3] J. Lee, J. Ham, H. Lee, W. Jang, H. Kim, B. So, and S. Ko, *Proc. 2024 IEEE International Solid-State Circuits Conference (ISSCC)* (IEEE, San Francisco, USA, 2024) p. 43.
doi: https://doi.org/10.1109/ISSCC49657.2024.10454341

[4] K. H. Lee, S. P. Nam, J. H. Lee, M. Choi, H. J. Ko, S. H. Byun, J. C. Lee, Y. H. Lee, Y. C. Rhee, Y. K. Choi, B. H. Kang, C. B. Park, S. Park, and T. Kim, Proc. 2018 IEEE International Solid-State Circuits Conference - (ISSCC) (IEEE, San Francisco, USA, 2018) p. 184.
doi: https://doi.org/10.1109/ISSCC.2018.8310245

[5] M. Miyamoto, M. Hamaguchi, and A. Nagao, *IEEE J. Solid-State Circuits*, **50**, 335 (2015).
doi: https://doi.org/10.1109/JSSC.2014.2364092

[6] Y. H. Yu and T. Y. Sun, *IEEE Sens. J.*, **16**, 390 (2016).
doi: https://doi.org/10.1109/JSEN.2015.2479599

[7] M. Hamaguchi, M. Takeda, and M. Miyamoto, *Proc. 2015 IEEE International Solid-State Circuits Conference - (ISSCC) Digest of Technical Papers* (IEEE, San Francisco, USA, 2015) p. 1.
doi: https://doi.org/10.1109/ISSCC.2015.7062955

[8] K. H. Seol, S. Park, J. Lee, and H. Nam, *J. Soc. Inf. Disp.*, **28**, 831 (2020).
doi: https://doi.org/10.1002/jsid.921

[9] C. B. Park, S. S. Park, K. D. Kim, S. H. Park, J. W. Park, B. H. Kang, Y. H. Huh, G. H. Cho, *IEEE Journal of Solid-State Circuits*, **51**, 168 (2016).
doi: https://doi.org/10.1109/JSSC.2015.2453943

[10] J. S. An, S. H. Han, J. E. Kim, D. H. Yoon, Y. H. Kim, H. H. Hong, J. H. Ye, S. J. Jung, S. H. Lee, J. Y. Jeong, K. H. Baek, S. K. Hong, and O. K. Kwon, *Proc. 2017 IEEE International Solid-State Circuits Conference (ISSCC)* (IEEE, San Francisco, USA, 2017) p. 168.
doi: https://doi.org/10.1109/ISSCC.2017.7870314

[11] J. S. An, J. H. Ra, E. Kang, M.A.P. Pertijs, and S. H. Han, *Proc. 2020 IEEE International Solid-State Circuits Conference - (ISSCC)* (IEEE, San Francisco, USA, 2020) p. 430.
doi: https://doi.org/10.1109/ISSCC19947.2020.9063020

[12] J. S. An, S. H. Han, K. B. Park, J. E. Kim, J. H. Ye, S. H. Lee, J. Y. Jeong, J. S. Kim, K. H. Baek, K. S. Chung, S. K. Hong, and O. K. Kwon, *Proc. 2018 IEEE International Solid-State Circuits Conference - (ISSCC)* (IEEE, San Francisco, USA, 2018) p. 182.
doi: https://doi.org/10.1109/ISSCC.2018.8310244

[13] M. Hamaguchi, A. Nagao, and M. Miyamoto, *Proc. 2014 IEEE International Solid-State Circuits Conference Digest of Technical Papers (ISSCC)* (IEEE, San Francisco, USA, 2014) p. 214.
doi: https://doi.org/10.1109/ISSCC.2014.6757405

[14] H. Shin, S. Ko, H. Jang, I. Yun, and K. Lee, *Proc. 2013 IEEE International Solid-State Circuits Conference Digest of Technical Papers* (IEEE, San Francisco, USA, 2013) p. 388.
doi: https://doi.org/10.1109/ISSCC.2013.6487782

[15] S. I. Yoshida, M. Hamaguchi, T. Morishita, S. Shinjo, A. Nagao, and M. Miyamoto, *Proc. 2014 IEEE Asian Solid-State Circuits Conference (A-SSCC)* (IEEE, KaoHsiung, Taiwan, 2014) p. 217.
doi: https://doi.org/10.1109/ASSCC.2014.7008899